Combinatorial Mixture Models for Single Cell Assays with Application to Vaccine Studies

Greg Finak[1], SC De Rosa[2], Mario Roederer[3], and Raphael Gottardo[1]

[1]Vaccine and Infectious Disease Division, Fred Hutchinson Cancer Research Center (FHCRC), Seattle, WA
[2]HIV Vaccine Trials Network, Fred Hutchinson Cancer Research Center (FHCRC), Seattle, WA
[3]Vaccine Research Center, NIAID, NIH, 40 Convent Drive, Rm 5509, Bethesda, MD 20892

June 29, 2012

Abstract

Immunological endpoints in vaccine trials are measured through a variety of assays that provide single–cell measurements of multiple genes and proteins in specific immunological cell populations. Using single–cell data, we consider the problem of identifying subjects where these cell populations exhibit differential responses under different experimental conditions. For example, in the intracellular cytokine staining assay from flow cytometry, individual cells are classified as either positive or negative for a marker based on a predetermined threshold. The assay is used to assess an individual's immune response to a vaccine by measuring the number of antigen–specific cells producing different cytokines in different T–cell subpopulations in response to different antigen stimulations. Individuals whose T–cells exhibit increased production of a cytokine in response to stimulation are termed "positive" for that cytokine, and multiple such "positivity calls" are used to identify vaccine responders. Here we present a framework based on mixtures of Beta–binomial or Dirichlet–Multinomial distributions for analyzing count data derived from such single–cell assays. Our method models cellular responses in a marker–specific manner, treating the responding and non–responding observations as separate components in the model. Cell counts from the different experimental conditions are modelled independently, while sharing information across responding and non–responding observations through empirical Bayes priors in order to increase the sensitivity and specificity of positivity calls. We compare our method against Fisher's exact test, a likelihood ratio test, and ranked log fold changes, and show how it can be extended to model multivariate (multiple markers) cellular responses. In simulations and applied to real data sets, we find that our method has higher sensitivity and specificity than Fisher's exact test and alternative methods.

1 Introduction

In the 1970s, single-cell analysis was revolutionized with the development of fluorescence-based flow cytometry (FCM). Since then, instrumentation and reagent advances have enabled the study of numerous cellular processes via the simultaneous single cell measurement of multiple surface and intracellular markers (up to 17 markers). More recent technological development have drastically extended the capabilities of single-cell cytometry to measure dozens of simultaneous parameters per cell. Although cells sorted using well-established surface markers may appear homogeneous, mRNA expression of other genes within these cells can be heterogeneous4,5 and could further characterize cell poly-functionality. A new technology based on microfluidic arrays combined with multiplexed polymerase chain reactions (PCR) can now be used to perform thousands of PCRs in a single device, enabling simultaneous, high-throughput gene expression measurements at the single-cell level across hundreds of cells and genes6. While classic gene expression microarrays sum the expression from many individual cells, the intrinsic stochastic nature of biochemical processes results in relatively large cell-to-cell gene expression variability. This heterogeneity may carry important information, thus single cell expression data should not be analyzed in the same fashion as cell-population level data. Special treatment of single cell level data, which preserves information about population heterogeneity, is warranted in general. For this reason, single–cell assays are an important tool in immunology, providing a functional and phenotypic snapshot of the immune system at a given time. These assays typically measure multiple variables simultaneously on individual cells in a heterogeneous mixture such as whole blood. These variables are used to classify individual cells in the mixture into more homogeneous sub–populations based on phenotypic or functional differences. Such single–cell assays are used for immune monitoring of disease, vaccine research, and diagnosis of haematological malignancies [1–3].

A motivating example from vaccine research is the flow cytometric intracellular cytokine staining (ICS) assay, which is used to identify and quantify individuals' immune responses to a vaccine. Upon vaccination, antigen in the vaccine is taken up and presented to CD4 or CD8 T–cels via antigen presenting cells. While not all T–cells can recognize all antigens, those that recognize antigens in the vaccine become *activated* and produce a variety of cytokines, further promoting the immune response. After activation, this antigen–specific subpopulation proliferates and can persist in the immune system for some time providing *memory* that can more rapidly recognize the same antigen again in the future [4]. These antigen–specific T–cell subpopulations constitute a very small fraction of the total number of CD4 and CD8 T–cells. The ICS assay measures the number of antigen–specific T–cells in whole blood by measuring cytokine production in response to activation following stimulation by an antigen that closely matches what was present in the original vaccine. Individual cells are labelled using fluorescently conjugated antibodies against phenotypic markers (CD3, CD4, and CD8) and functional markers (cytokines) of the cell subpopulations of interest [2, 5, 6]. A sufficiently large number of cells must be

collected to ensure that the rare cell populations can be detected. Subsequently, each individual cell is classified as either positive or negative for each maker based on predetermined thresholds, then the number of cells matching each subpopulation phenotype is counted. These counts are compared between antigen stimulated and unstimulated samples from an individual to identify significant differences. Assessing a broad T cell response to a vaccine is particularly important in HIV vaccine trials, where the search for immune correlates of protection against HIV progression and infection is ongoing [5, 7–9].

Although there is no standard approach to analyzing ICS assay data current methods range from ad–hoc rules based on log–fold changes, to permutation tests based on Hotelling's T^2 statistics, to exact tests of 2x2 contingency tables (e.g., Fisher's exact test and χ^2 test[1]) [5, 10–12, 14]. These methods generally test pairwise combinations of markers, raising questions of appropriate multiple testing adjustments, or they perform global tests of significance on multiple markers resulting in decreased power to detect small changes in subsets of cytokines [12, 13]. In the context of single-cell gene expression, very few methods have been proposed. To date, published analysis of Fluidigm data ignore cells where transcripts are undetected, focusing solely on continuous gene expression measurements. However, the proportion of single cells expressing individual genes also carries information and should be evaluated.

The framework developed in this paper addresses these issues explicitly. We present a multinomial-Dirichlet combinatorial mixture model framework for the analysis of single–cell assay data where multivariate measurement are made on individual cells. The model is used to identify observations where a significant difference exists between paired treatment and control samples with respect to the number of cells expressing different combinations of proteins, genes, or other measured properties of the cells. Importantly, our approach shares information across individuals (or subjects) by means of a Dirichlet prior distribution placed on the unknown cell population proportions of the mutinomial likelihood, which help increase sensitivity and specificity to detect rare antigen specific responding cell populations. The cell counts from the stimulated and unstimulated experiments are modeled independently, and different combinations of markers are represented as different mixture components in the framework. This approach allows us to omit certain combinations of markers that are not observable (i.e., two cytokines may never be co–expressed), or to explicitly represent combinations that are of interest (i.e., we can explicitly represent and test for a difference in a pair of cytokines in an experiment measuring many cytokines). This is a flexible approach that avoids the some of the drawbacks of global tests when only a few of the many measured markers show differences [12].

[1] make sure there is a reference for that. Added ref for the HVTN054 trial and the ICS standardization paper from Horton

2 Data structure and notation

In this paper we consider two different immunological single-cell assays typically used in vaccine trials, one flow cytometry data set, and one single-cell gene expression data set.

Flow cytometry: The primary ICS data set is from a trial testing the GeoVax DNA and MVA vaccines in a prime-boost regimen with 120 individuals (98 vaccines and 20 placebo recipients, see supplementary material S.1.1). The goal of this data set was to assess the immune response to the vaccine across multiple stimulations, time points, cytokines and T–cell subsets. Here, we analyzed the vaccinees (n=98) at two time points as a pooled data set (day 0 where no response is expected, and at day 182, the primary immunological endpoint).

Simulation studies were based on hyper parameter estimates from a dataset is from a phase-I (safety and efficacy) trial of an adenoviral vector vaccine in individuals without prior immunity, measuring four cytokines via intracellular cytokine staining (ICS) in two cell populations from 20 individuals at two time points (zero and 28 days post-vaccination, see supplementary material S.1.1 for details) [14]. The statistical analysis of ICS data in the published trial is described in the original manuscript and outlined in the supplementary information (supplementary material S.1.1) [14]. The goal of this data set was to assess and quantify response rates of CD4 and CD8 T-cell populations to different antigens.

Fluidigm single-cell gene expression: This is a single-cell gene expression data set of flow-sorted CD8–positivie T-cells from sixteen individuals. T-cells isolated by flow cytometry from sixteen individuals were stimulated in blocks of four individuals with four different antigens (HIV Gag, HIV Nef, CMV pp65 tm10, CMV pp65 nlv5) and gene expression post–stimulation measured at the single-cell level using the BioMark system (Fluidigm) 96×96 well arrays. The expression from the simulated samples was compared to paired, unstimulated controls. [2].

In the remainder of the paper, we use the following notation to describe our model. From this point on, we assume that we observe cell counts from I individuals in two conditions: stimulated and un-stimulated. Each cell can either be positive or negative for a marker. Given a set of K markers, the measured cells can be classified into 2^K positive/negative marker combinations. We denote by n_{sik} and n_{uik}, $k = 1 \dots 2^K$, the observed counts for the 2^K combinations in the stimulated and un-stimulated samples. We denote by $N_{si} = \sum_k n_{sik}$ and $N_{ui} = \sum_k n_{uik}$ the total number of cells measured for individual i in each sample. For ease of notations, we will denote by $\mathbf{y}_i$ the vector of observed counts for individual i, *i.e.* $\mathbf{y}_i = (\mathbf{n}_{si}, \mathbf{n}_{ui})$ where $\mathbf{n}_{si} = \{n_{sik} : k = 1, \dots, 2^K\}$ and $\mathbf{n}_{ui} = \{n_{uik} : k = 1, \dots, 2^K\}$. Finally, we define $\mathbf{y} = (\mathbf{y}_1, \dots, \mathbf{y}_I)$.

[2] Add a bit more info here, how many genes, tetramer sorted, etc, Mario et al. could you fill this in?

3 Differential expression with one marker

Datasets like the ones presented here are usually analyzed one marker at a times to avoid being underpowered due to the large number of combinations and the potential for very small cell counts in many of the combinations. As a consequence, we first consider the one marker case where cell counts are marginalized and each marker is analyzed separately and $K = 1$. In this case, for a given individual, the data can be summarized in a contingency table of $+/-$ cell counts across the un-stimulated and stimulated samples as depicted in Table 1.

Table 1: 2 x 2 contingency table of counts for marker positive and negative cells between stimulated (s) and unstimulated (u) conditions for a given individual i.

	Marker	
	Negative	Positive
Stimulated	$N_{si} - n_{si}$	n_{si}
Unstimulated	$N_{ui} - n_{ui}$	n_{ui}

For a given individual and stimulation, we consider a marker to be differentially expressed if the proportion of positive cells in the stimulated samples is different from the number of positive cells in the un-stimulated sample. Individuals that show differential expression for a given marker will be called responders for that marker. In this section, we shall be concerned with identifying differential expression one marker at a time, using a beta-binomial mixture model as described in what follows.

3.1 Beta-Binomial Model for One Marker

For a given individual i, the positive cell counts for the stimulated and un-stimulated samples are jointly modeled as follows,

$$(n_{si}|p_{si}) \sim \text{Bin}(N_{si}, p_{si}) \quad \text{and} \quad (n_{ui}|p_{ui}) \sim \text{Bin}(N_{ui}, p_{ui}) \tag{1}$$

where p_{si}, p_{ui} are the unknown proportions for the stimulated and un-stimulated paired samples. In order to detect responding individuals we consider two competing models:

$$\mathcal{M}_0 : p_{ui} = p_{si} \quad \text{and} \quad \mathcal{M}_1 : p_{ui} \neq p_{si}. \tag{2}$$

Under the null model, $\mathcal{M}_0$, there is no difference between the stimulated and un-stimulated samples, and the proportions are equal. Under the alternative model, $\mathcal{M}_1$, there is a difference in proportions between the two samples and the individual i is a responder.

3.2 Priors

Our model shares information across all individuals using exchangeable Beta priors on the unknown proportions, as follows,

$$(p_{ui}|z_i = 0) \sim \text{Beta}(\alpha_u, \beta_u) \tag{3}$$

$$(p_{si}|z_i = 1) \sim \text{Beta}(\alpha_s, \beta_s) \quad \text{and} \quad (p_{ui}|z_i = 1) \sim \text{Beta}(\alpha_u, \beta_u) \tag{4}$$

where z_i is an indicator variable equal to one if individual i is a responder, i.e. $\mathcal{M}_1$ is true, and zero otherwise, and $\alpha_u, \beta_u, \alpha_s, \beta_s$ are unknown hyper-parameters shared across all individuals. Note that the parameters α_u, β_u are explicitly shared across the two models, whereas α_s, β_s are only present in the alternative model. Finally, we assume that the z_i's are independent and identically distributed Bernoulli with probability w, where w represents the proportion of responders. It follows that marginally, *i.e.* after integrating z_i, p_{ui} and p_{si} are jointly distributed as a mixture of a one dimensional and a two dimensional Beta distributions with mixing parameter w. Treating the z_i's as missing data, the unknown parameter vector $\boldsymbol{\theta} \equiv (\alpha_u, \beta_u, \alpha_s, \beta_s, w)$ can be estimated in an Empirical-Bayes fashion using and Expectation-Maximization [15] algorithm as described in Section 3.3. As an alternative, we will also explore a fully Bayesian model where the hyperparameters α_u, β_u and α_s, β_s are given vague exponential priors with mean 10^3, and w is assumed to be drawn from a uniform distribution between 0 and 1. In this case, all parameters will be estimated via a Markov Chain Monte Carlo algorithm as described in Section 3.3.

3.3 Parameter estimation

Our estimation algorithms make direct use of the marginal likelihoods, L_0 and L_1, obtained after integrating out the $p_{\{s,u\}i}$'s for the null and alternative models, to simplify our calculations. Given the conjugacy of the priors, the marginal likelihoods L_0 and L_1 are available in closed forms (supplementary material), and are given by,

$$\text{L}_0(\alpha_u, \beta_u|\mathbf{y}) = \prod_{i=1}^{P} \binom{N_{ui}}{n_{ui}} \binom{N_{si}}{n_{si}} \frac{\text{B}(n_{si} + n_{ui} + \alpha_u, N_{si} - n_{si} + N_{ui} - n_{ui} + \beta_u)}{\text{B}(\alpha_u, \beta_u)} \tag{5}$$

and

$$\text{L}_1(\alpha_u, \beta_u, \alpha_s, \beta_s|\mathbf{y}) = \prod_{i=1}^{P} \binom{N_{ui}}{n_{ui}} \binom{N_{si}}{n_{si}} \frac{\text{B}(n_{ui} + \alpha_u, N_{ui} - n_{ui} + \beta_u)}{\text{B}(\alpha_u, \beta_u)} \frac{\text{B}(n_{si} + \alpha_s, N_{si} - n_{si} + \beta_s)}{\text{B}(\alpha_s, \beta_s)}. \tag{6}$$

Assuming that the missing data, the z_i's, are known, we define the complete log-likelihood as follows,

$$l(\boldsymbol{\theta}|\mathbf{y}, \mathbf{z}) = \sum_i z_i l_0(\alpha_u, \beta_u|\mathbf{y}_i) + (1-z_i) l_1(\alpha_u, \beta_u, \alpha_s, \beta_s|\mathbf{y}_i) + z_i \log(w) + (1-z_i) \log(1-w) \tag{7}$$

where l_0 and l_1 are the log marginal-likelihoods and $\boldsymbol{\theta} \equiv (\alpha_u, \beta_u, \alpha_s, \beta_s, w)$ is the vector of parameters to be estimated.

3.3.1 EM algoritm

Given an estimate of the model parameter vector $\tilde{\boldsymbol{\theta}} = \left\{\tilde{\alpha}_u, \tilde{\beta}_u, \tilde{\alpha}_s, \tilde{\beta}_s, \tilde{w}\right\}$ and the data $\mathbf{y}$, the E step consists of calculating the posterior probabilities of differential expression, defined by

$$\tilde{z}_i \equiv \Pr(z_i = 1|\mathbf{y}, \tilde{\boldsymbol{\theta}}) = \frac{\tilde{w} \cdot \mathrm{L}_1(\tilde{\alpha}_u, \tilde{\beta}_u, \tilde{\alpha}_s, \tilde{\beta}_s, |\mathbf{y}_i)}{(1-\tilde{w}) \cdot \mathrm{L}_0(\tilde{\alpha}_u, \tilde{\beta}_u|\mathbf{y}_i) + \tilde{w} \cdot \mathrm{L}_1(\tilde{\alpha}_u, \tilde{\beta}_u, \tilde{\alpha}_s, \tilde{\beta}_s|\mathbf{y}_i)}.$$

The M-step then consist of optimizing the complete-data log-likelihood over $\boldsymbol{\theta}$ after replacing z_i by $\tilde{z}_i$ in (7). Straightforward calculations lead to $\tilde{w} = \sum_i \tilde{z}_i / I$, but unfortunately no closed form solutions exist for the remaining parameters. We use numerical optimization as implemented in R's *optim* function to estimate the remaining parameters. Starting from some initial values, the EM algorithms iterates between the E and M steps until convergence. In our case, we initialize the z_i's using Fisher's exact test to assign each observation to either the null or alternative model components. We then use the estimated z_i's to estimate the p_{ui}'s and p_{si}'s and use these to set the hyper-parameters to their method-of-moments estimates.

3.3.2 MCMC algorithm

Realizations were generated from the posterior distribution via MCMC algorithms [16]. All updates were done via Metropolis-Hastings sampling except for the z_i's and w that were done via Gibbs samplings. Details about the algorithms are given in supplementary material. We used the method of Raftery and Lewis [17, 18] to determine the number of iterations, based on a short pilot run of the sampler. For each dataset presented here, this suggested that a sample of no more than about 1,000,000 iterations with 50,000 burn-in iterations was sufficient to estimate standard posterior quantities. Guided by this, and leaving some margin, we used 2,000,000 iterations after 50,000 burn-ins for each dataset explored here.

4 Results

The constrained model was applied to an ICS data set from a real–world vaccine trial in order to identify responders to antigen stimulation. The unconstrained model was applied to Fluidigm single–cell gene expression data to identify genes differentially expressed between stimulated and unstimulated conditions in populations of single–cells. We also performed simulation studies to assess the performance of the constrained and unconstrained models in a univariate and multivariate settings.

4.1 ICS

MIMOSA Outperforms Competing Methods on Vaccine Trial Data from Study HVTN065

We tested our method on ICS data from HVTN065, a trial testing the GeoVax DNA and MVA vaccines in a prime-boost regimen, with 120 individuals (98 vaccines and 20 placebo recipients). We analyzed the vaccinees (n=98) at the day 0 and day 182 (the primary endpoint) time points as a pooled data set. Observations at the day 0 time point were treated as true negatives, while observations at the day 182 time point were treated as true positives (potentially underestimating the sensitivity). We examined the CD4+ T–cell cytokine responses for ENV-1-PTEG and GAG-1-PTEG stimulated samples. An ROC (receiver operator characteristic) analysis was performed to assess the sensitivity and specificity of the constrained MIMOSA model compared to Fisher's exact test, ranked log fold change, and a likelihood ratio test based on the MIMOSA model for identifying vaccine responders and non–responders.

The MMOSA model had higher sensitivity and specificity than Fisher's exact test, the likelihood ratio test, or ranked log fold change for discriminating vaccine responders and non–responders when the magnitude of response was small (i.e. ENV-1-PTEG stimulation) (Figure 1 A), (AUC=0.954 for MIMOSA vs. 0.923 for Fisher's exact test vs. 0.827 for LRT vs. 0.775 for ranked fold change). When the magnitude of response was larger (GAG-1-PTEG stimulation), MIMOSA performed as well as Fisher's exact test, and better than other competing methods (Figure 1 C) (AUC=0.982 for MIMOSA vs. 0.978 for Fisher's exact test vs. 0.877 for LRT vs. 0.784 for ranked fold change). Irrespective of the magnitude of the response to stimulation, MIMOSA gave better estimates of the observed false discovery rate than competing methods (Figure 1 B,D). These results are consistent for other cytokines (see supplementary material S.1.2, supplementary figures 1 and 2).

4.2 Fluidigm

4.2.1 MIMOSA Identifies Stimulation-Specific Patterns of Gene Expression in Fluidigm Single–Cell Data

We applied the MIMOSA model to Fluidigm single–cell gene expression data from CD8+ T–cells from 16 individuals, under four different stimulation conditions, as well as unstimulated samples. The unconstrained MIMOSA model was fit to each stimulation. From the model we calculated the posterior probabilities of response for each gene, the posterior differences in the proportion of cells expressing each gene between stimulated and unstimulated conditions, as well as the posterior log ratio of the proportion of cells expressing each gene in stimulated and unstimulated conditions. The data are presented in (Figure 2 A-C). Importantly, we see that MIMOSA identifies stimulation–specific differences in the proportions of cells expressing each gene, while preserving inter–subject variability (Figure 2).

These patterns are evident in the posterior probabilities (Figure 2 A), and preserved in the posterior estimates of the differences of proportions and the posterior log fold changes of proportions(Figure 2 B,C).

4.3 Simulation Studies

We examined the performance of the constrained ($p_s > p_u$) and unconstrained ($p_s \neq p_u$) beta–binomial mixture models via simulations. Using hyper parameters estimated from the constrained model fit to data from Gag1–stimulated, CD4–positive, IL2–expressing T–cells from day 28 post–vaccination of the HVTN054 trial [14]. We simulated data from this constrained model with 500 observations, a response rate of 60%, an N of 10K, 20K, 30K, 50K, 75K, 100K, and 150K events, with ten independent realizations of data for each N. Constrained MIMOSA was fit to this data and the sensitivity and specificity of the model's ability to correctly identify observations from the "responder" and "non–responder" components was evaluated through analysis of ROC curves, and compared against Fisher's exact test, the likelihood ratio test, and ranked log fold change. This procedure was repeated for the unconstrained model fit to unconstrained data (Figure 3 A-D). The nominal vs observed false discovery rate was also examined to assess the model fit (Figure 3 E-F).

For both the constrained and unconstrained simulations, MIMOSA out–performed competing methods, including Fisher's exact test, with respect to sensitivity and specificity at all values of N (Figure 3 A, D). Additionally, the false discovery rate for MIMOSA more closely reflected the nominal false discovery rate compared to Fisher's exact test (Figure 3 E, F).

To assess the sensitivity of the model to deviations from model assumptions, we repeated the simulations with the cell proportions drawn from truncated normal distributions on $(0, 1)$, rather than beta distributions. The means and variances of the truncated normal distributions were set to the maximum likelihood estimates of the beta distributions defined by the α, β hyper parameters estimated from the HVTN065 data set (Figure 4). Even under these departures from the model assumptions, the unconstrained MIMOSA model outperformed Fisher's exact test and performed about as well as the constrained MIMOSA model fit to one-sided data.

5 Differential expression across marker combinations

Our beta-binomial model described in section 3.1 can be generalized to a Dirichlet-multinomial model to assess differential expression across multiple marker combinations. As described in the data section, we now have counts for each marker combination, denoted by $\mathbf{n}_{si} = \{n_{sik} : k = 1, \ldots, 2^K\}$ and $\mathbf{n}_{ui} = \{n_{uik} : k = 1, \ldots, 2^K\}$.

5.1 Model

In our multivariate model, the beta distribution is replaced by a multinomial distribution, as follows,

$$(\mathbf{n}_{ui}|\mathbf{p}_{ui},) \sim \mathcal{M}(N_{ui}, \mathbf{p}_{ui}) \quad \text{and} \quad (\mathbf{n}_{si}|\mathbf{p}_{si}) \sim \mathcal{M}(N_{si}, \mathbf{p}_{si}) \tag{8}$$

where $N_{\{s,u\}i} = \sum_{k=1}^{2^K} n_{\{s,u\}ik}$ are the number of cells collected and $\mathbf{p}_{ui}$ and $\mathbf{p}_{si}$ are the unknown proportions for the un-stimulated and stimulated samples.

5.2 Prior

As in the one-marker case, we share information across subjects using an exchangeable prior on the unknown proportions. This time the beta priors are replaced by Dirichlet priors, as follows,

$$\begin{aligned} &(\mathbf{p}_{ui}|z_i = 0) \sim \mathrm{Dir}(\boldsymbol{\alpha}_u) \\ &(\mathbf{p}_{ui}|z_i = 1) \sim \mathrm{Dir}(\boldsymbol{\alpha}_u) \quad \text{and} \quad (\mathbf{p}_{si}|z_i = 1) \sim \mathrm{Dir}(\boldsymbol{\alpha}_s) \end{aligned} \tag{9}$$

where the indicator variable z_i is as defined in (2), i.e. $z_i \sim \mathrm{Be}(w)$ where w is the proportion of responders. As in the beta-binomial case both an EM and MCMC algorithms can be used for parameter estimation. When using a fully Bayesian approach via MCMC, we use the same priors for $\boldsymbol{\alpha}_{\{u,s\}}$ and w as for the beta-binomial model.

5.3 Parameter estimation

Again, to simplify the estimation problem, we make use of the marginal likelihoods that can be obtained in closed forms (see supplementary material). For the null component, the marginal likelihood L_0 is given by,

$$\mathrm{L}_0(\boldsymbol{\alpha}_u|\mathbf{n}_s, \mathbf{n}_u) = \prod_{i=0}^{I} \frac{\mathrm{B}(\boldsymbol{\alpha}_u + \mathbf{n}_{ui} + \mathbf{n}_{si})}{\mathrm{B}(\boldsymbol{\alpha}_u)} \cdot \frac{N_{si}!}{\prod_k n_{sik}!} \cdot \frac{N_{ui}!}{\prod_k n_{uik}!} \tag{10}$$

where B is the 2^K-dimensional Beta function defined as $\mathrm{B}(\boldsymbol{\alpha}) = \prod_k \Gamma(\alpha_k)/\Gamma(\sum_k \alpha_k)$. Similarly the marginal likelihood for the alternative model is given by

$$\mathrm{L}_1(\boldsymbol{\alpha}_u, \boldsymbol{\alpha}_s|\mathbf{n}_s, \mathbf{n}_u) = \prod_{i=0}^{I} \frac{\mathrm{B}(\boldsymbol{\alpha}_u + \mathbf{n}_{ui})\mathrm{B}(\boldsymbol{\alpha}_s + \mathbf{n}_{si})}{\mathrm{B}(\boldsymbol{\alpha}_s)\mathrm{B}(\boldsymbol{\alpha}_u)} \cdot \frac{N_{si}!}{\prod_k n_{sik}!} \cdot \frac{N_{ui}!}{\prod_k n_{uik}!}. \tag{11}$$

The estimation procedures (both EM and MCMC based) for the multinonial-Dirichlet are the same as for the beta-binomial model except that the number of parameters to be estimated is larger. In our experience, the performance of the EM algorithm greatly deteriorates when K becomes larger than 2. The EM algorithms becomes very dependent

on the initial values, and can even fail to converge when good initial values are provided. Although our MCMC algorithm is slightly more computational, it does not suffer from this problem and can be used even when K is large. More details about both algorithms are given in supplementary material.

5.3.1 Polyfunctionality in Fluidigm Single Cell Gene Expression Data

We fit the multivariate MIMOSA model to the two–sided Fluidigm data, looking at coexpression of pairs of genes in single cells across the four stimulations. In Figure 5 we show heatmaps of the counts of cells expressing all combinations of the BIRC3 and CCL5 genes in unstimulated and stimulated samples (Figure 5 A,B). Only CCL5 positive cells express BIRC3, and the expression of BIRC3 increases upon stimulation. The typical approach to analyzing polyfunctional populations from intracellular cytokine staining data (summing the counts over all possible polyfunctional cell populations) would not be appropriate in this case, since changes in the counts of these different cell populations occur in both directions. That is to say, the number of BIRC3-/CCL5+ cells decreases upon stimulation and the number of BIRC3+/CCL5+ cells increases. There is no difference in the marginal counts for any sample (Figure 5 C). In contrast, multivariate MIMOSA tests all cell subpopulations simultaneously, and identifies a significant difference between stimulated and unstimulated conditions in 13 of the 16 samples (Figure 5 D). Testing all combinations simultaneously is an advantage over performing multiple univariate tests on the individual combinations, which requires multiplicity adjustment and a potential loss of power.

Since the Fluidigm data has a limited number of observations (100 cells and 16 samples), we performed simulations (five–dimensional data) to assess the power of the multivariate MIMOSA model compared to Fisher's exact test on the resulting 2x5 tables, Fisher's exact test performed marginally on each dimension of the data and p–values combined through Fisher's method ($\chi^2 = -2\sum_{i=1}^{k}\log(p_i)$), as well as the likelihood ratio test (Figure 6 A-C). These results show that multivariate MIMOSA has significantly increased power to detect true differences in multivariate data, even with small counts and small effect sizes, and the model is a better fit to the data than other standard approaches tested for analyzing such multivariate count data (Figure 6 B).

6 Discussion

The variety of single–cell assays being adopted by the immunology community is increasing. Flow cytometry, mass cytometry, ELISPOT, Fluidigm, and other single–cell assays can all be analyzed as single–cell count data. Development of effective statistical methods to detect differences in gene or protein expression at the single cell level is becoming increasingly important. Current approaches rely on asymptotic approximations (t–test, or χ^2 test), empirical or ad–hoc methods (2–fold change), or exact tests (Fisher's exact test) where model assumptions are generally not satisfied, all of which can lead to invalid conclusions

about the data [5, 10, 11, 13, 19]. Most importantly, existing classical methods do not share information across samples, resulting in less power to detect true differences than empirical-Bayes and hierarchical modelling approaches, which are widely applied in the microarray literature [20–22].

The MIMOSA model presented here uses a mixture model framework of Beta–Binomial or Multinomial–Dirichlet distributions to model counts in experimental units (i.e. individuals) across multiple conditions (i.e. vaccine responders and non–responders). Information is shared across non–responder individuals and across responders individuals through exchangeable Beta or Dirichlet priors, increasing the power to detect true differences between treatment and control conditions compared to Fisher's exact test, even when model assumptions are violated (Figures 3 and 4). The MIMOSA model based on the Beta–Binomial distribution allows us to constrain the alternative hypothesis to the case $p_s > p_u$, where the proportion of cells in the stimulated sample is strictly greater than the proportion of cells in the matched unstimulated sample.

Importantly, the analysis of real–world ICS data from vaccine trials demonstrated that the the constrained MIMOSA model performs as well or better than Fisher's exact test or other non-Bayesian alternatives for identifying vaccine responders across multiple antigen stimulations and multiple cytokines (Figure 1). Although the MIMOSA model was fit within each antigen stimulation $\times$ cytokine combination, the model is naive to vaccine time point. Despite this, MIMOSA demonstrated a higher sensitivity and specificity to discriminate between vaccine responders and non-responders on days 0 (pre–vaccination) and 182 (post–vaccination) than the current standard approach (Fisher's exact test), or non–Bayesian alternatives such as the likelihood ratio test or ranking by log–fold change (Figure 1 A,C). Our approach treats all day 0 observations as true negatives and all day 182 observations as true positives, yet we know that not all vaccine recipients are likely to exhibit a vaccine response on day 182. None the less, this shortcoming, at worst, leads us to underestimate the true sensitivity of MIMOSA, and does not negatively impact the comparison. Additionally, MIMOSA was found to be a better fit to real–world ICS data from vaccine trials than other analysis approaches, as evidenced by more accurate estimates of true false discovery rate (Figure 1 B,D).

Although ICS is the motivating example for the MIMOSA model, it can be applied any type of single–cell assay where cells are dichotomized into positive and negative sets, counted and compared across different conditions. To date, the typical approach to Fluidigm single cell gene expression analysis has been focused on identifying differences in the continuous part of the signal, corresponding to the C_t values and the "missing" data from cells that don't express a given gene has generally been ignored, or used as part of ad–hoc pre-filtering[23]. The ability of MIMOSA to identify stimulation–specific expression patterns in single–cell gene expression data demonstrates not only the broader utility of the method, but importantly, also demonstrates that biologically relevant signal is present in the proportion of cells expressing each gene under different conditions (Figure 2 A-C). MIMOSA explicitly models and performs inference on the observed positive cell counts be-

tween different conditions. Additionally, extending the model to take into account multiple conditions is straightforward.

Detecting differences in polyfunctional cell populations (i.e. identifying changes in cell populations that co–express multiple proteins, cytokines, or genes), is important in vaccine research, since it allows the identification of more precisely defined, more homogeneous cell popualtions [24]. These polyfunctional cell populations may be correlated with differential vaccine response or efficacy and have the potential to inform vaccine development and trial design. What's more, changes in these polyfunctional cell populations are not always detectable when looking at the marginal populations (Figure 5 A-C). Existing methods for identifying polyfunctional cytokine profiles from ICS data either separately test individual combinations of cytokines, or perform global tests between groups of individuals even when the populations under study are known to be heterogeneous (i.e. mixtures of responders and non–responders). Sometimes these tests are entirely empirical in nature (i.e. thresholds based on fold change or some factor over background), and these methods generally do not share information across observations [5, 10–13, 19]. As others have pointed out, in order to have the most power to detect a true difference, the statistical test should be selected taking into account the cytokine combinations of interest [12]. Here we have shown that MIMOSA has higher sensitivity and specificity than these competing methods to identify true differences between conditions in multivariate count data (Figure 5 A, and Figure 6 A,C), and the model generally provides a better fit to the single–cell assay count data arising from studies with these types of experimental designs (Figure 6 B).

7 Conclusions

We have developed a mixture model framework that we call MIMOSA .for identifying differences between treatment conditions in paired observations of cell counts from a variety of single–cell assays that frequently arise in the context of vaccine trials and immunological studies. Our model can be applied in a univariate or multivariate fashion, and we have shown that it has greater sensitivity and specificity than other typical approaches used to analyze the type of count–based data derived from single cell assays, including Fisher's exact test, the non-Bayesian likelihood ratio test, or ad–hoc rank based approaches. The software is implemented in R and C++, and is freely available from GitHub (`http://www.github.org/finak/MIMOSA`).

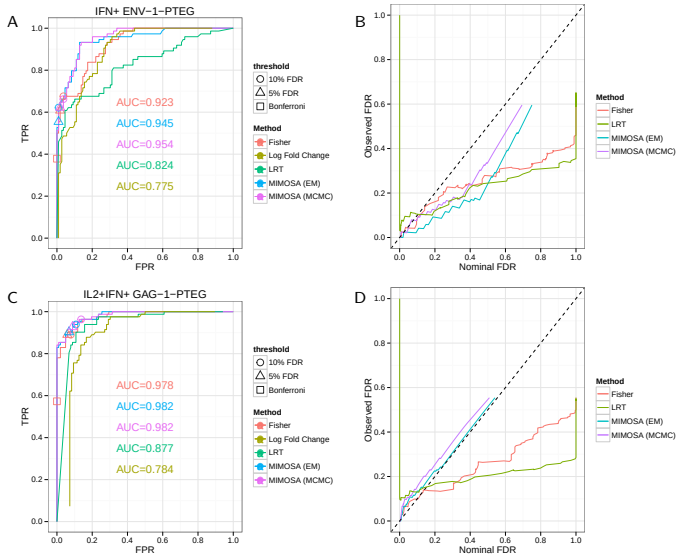

Figure 1: Performance of MIMOSA (EM and MCMC implementations, one–sided model) and competing methods on ICS data from HVTN065. Sensitivity and specificity (ROC analysis) as well as observed and nominal false discovery rates for positivity calls from CD4+ T–cells stimulated with A–B) ENV-1-PTEG and expressing IFNg or C–D) GAG-1-PTEG and expressing IL2 and IFNg. ROC and FDR plots of other cytokine combinations can be found in the supplementary material.

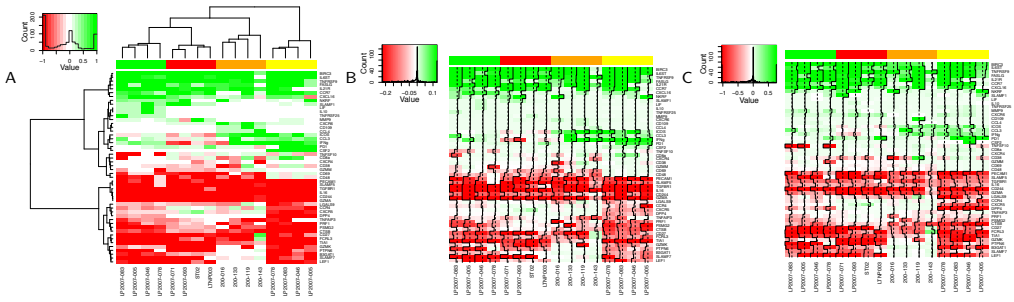

Figure 2: Signed posterior probability, difference and log-odds ratio of the proportion of single cells expressing each gene on a 96x96 Fluidigm array. The posterior probability of response times the sign of the change in expression is shown in A) (red indicates a significant decrease, green a significant increase, relative to the control). Columns and rows are clustered based on these signed posterior probabilities. B) The log_2 ratio of the proportion of cells expressing a gene in the stimulated vs. control samples. Rows and columns are ordered as in A) for comparison. C) The difference in the proportion of cells expressing each gene in the stimulated vs. control samples. Ordering of the rows and columns is preserved as in A). The traces show the deviations of each cell from zero. Colors along the columns denote different stimulations (green: CMV pp65 nlv5, red: HIV Gag, orange: HIV Nef, yellow: CMV pp65 tm10).

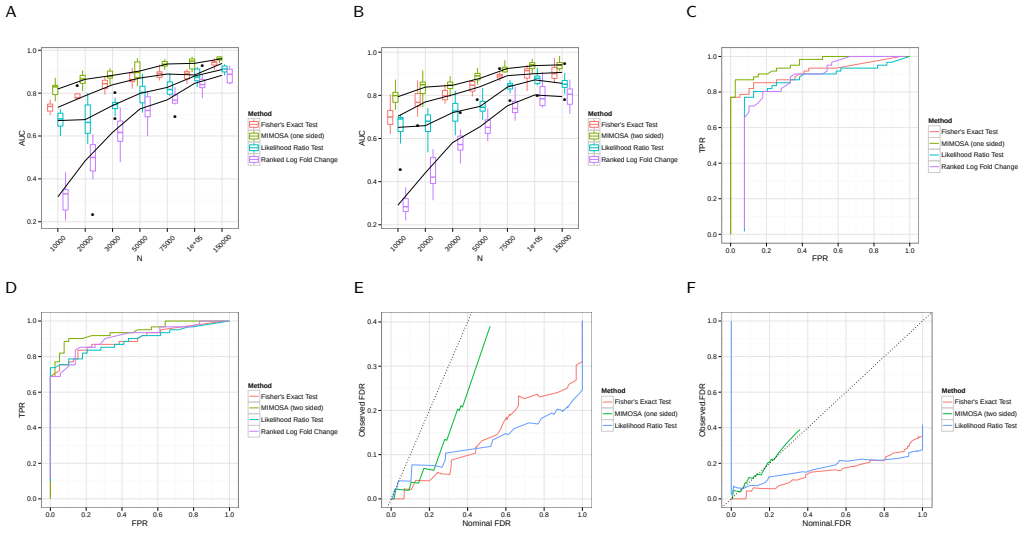

Figure 3: Comparison of positivity detection methods on data simulated from the one–sided model (top row) and the two–sided model (bottom row). Ten simulations were generated at each of seven increasing values of N (total counts) using hyper–parameter estimates from real ICS data. A) Boxplots of the area under the ROC curves for Fisher's exact test, MIMOSA (MCMC constrained model), likelihood ratio test, and the ranked log fold change. B) Boxplots for the unconstrained model. C) Observed and nominal false discovery rate for a representative simulated data set (N=100,000 counts) MIMOSA (one–sided), Fisher's exact test, and the likelihood ratio test. C) ROC curves for a representative simulated data set (N=100,000 counts). D) AUC boxplots, E) observed vs. nominal FDR, F) ROC analysis comparing MIMOSA (MCMC unconstrained model) and competing methods for two–sided simulated data.

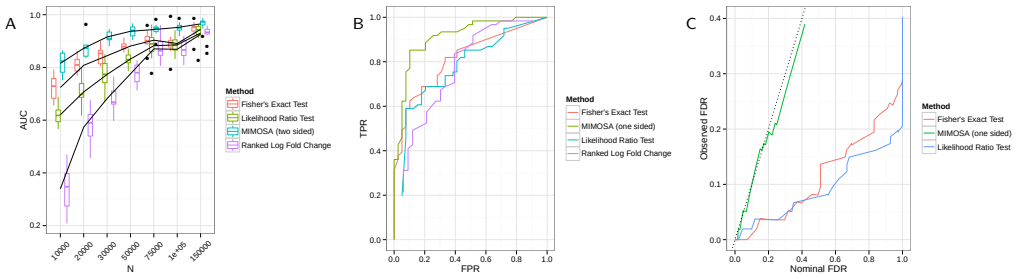

Figure 4: Unconstrained MIMOSA model fit to data where model assumptions are violated. Two–sided data were simulated from a model where the proportions were drawn from a truncated normal distribution over $[0, 1]$, rather than a Beta distribution.

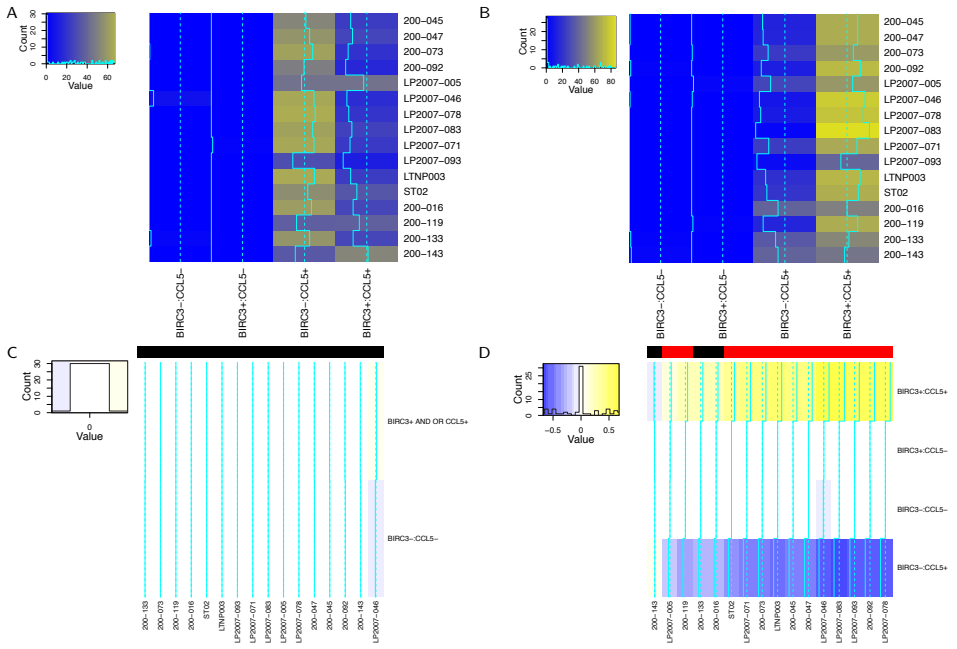

Figure 5: Counts of cells expressing different combinations of BIRC3 and CCL5 genes in the A) unstimulated and B) stimulated conditions. The posterior difference in proportions between stimulated and unstimulated samples fitting the C) marginalized counts D) multivariate combinations. No difference is observed from the marginalized counts, while multivariate MIMOSA detects a difference between stimulated and unstimulated conditions in 13 of 16 samples.

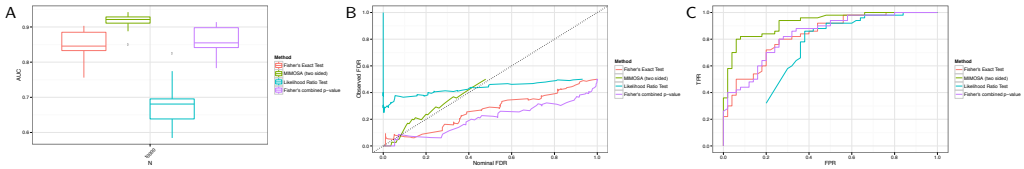

Figure 6: Multivariate simulations from a two–sided model. Ten, five-dimensional data sets were simulated from a two–sided model with an effect sizes of 2.5×10^{-3} and -2.5×10^{-3} in two of the five dimensions. Multivariate MIMOSA was compared against Fisher's exact test, the likelihood ratio test, and Fisher's combined p–value, combining Fisher's exact test run marginally on each of the five dimensions. A) Boxplots of AUCs (area under the curve) for the ten simulations. B) Observed and nominal false discovery rate for each method. C)ROC curves for the competing methods.

Supplementary Information

S.1.1 HVTN065 and HVTN054 Vaccine Trial ICS Data Description

HVTN065 is a phase 1 (safety and immunogenicity) trial of GeoVax HIV/AIDS DNA and MVA vaccine in 120 individuals (100 vaccinees, 20 placebo recipients, parts A and B). CD4 and CD8 T–cell epitope specific immune responses were measured via the ICS assay. Other humoral and cellular immune responses were measured via ELISA, and neutralizing antibody assays. Cytokines measured in the ICS assay included IFNg, TNFa, IL2, and IL4, and antigens included three Env, three Gag, and three Pol peptide pools. Results of the trial have been published [25].

HVTN054 is a phase 1 (safety and immunogenicity) trial of an adenoviral vector vaccine in individuals without prior immunity [14]. The vaccine vector expressed Gag, Pol and Env proteins from multiple HIV clades [14]. Vaccine was given at two increasing doses, as well as a placebo. T–cell responses to antigens in the vaccine were measured via the ICS assay [5, 14]. The cytokines measured were IFNg (Interferon–γ), IL2 (Interleukin–2), TNFa (Tumor necrosis factor–α) and IL4 (Interleukin 4) [5]. The sample size consisted of 20 vaccine and four placebo recipients. The original statistical analysis of the positivity calls is described in the associated publication [14]. The Gag stimulated, IL2 expressing, CD4+ T–cell data from day 28 was used to derive hyper–parameter estimates for the simulation studies.

S.1.2 HVTN065 Results for Other Cytokines

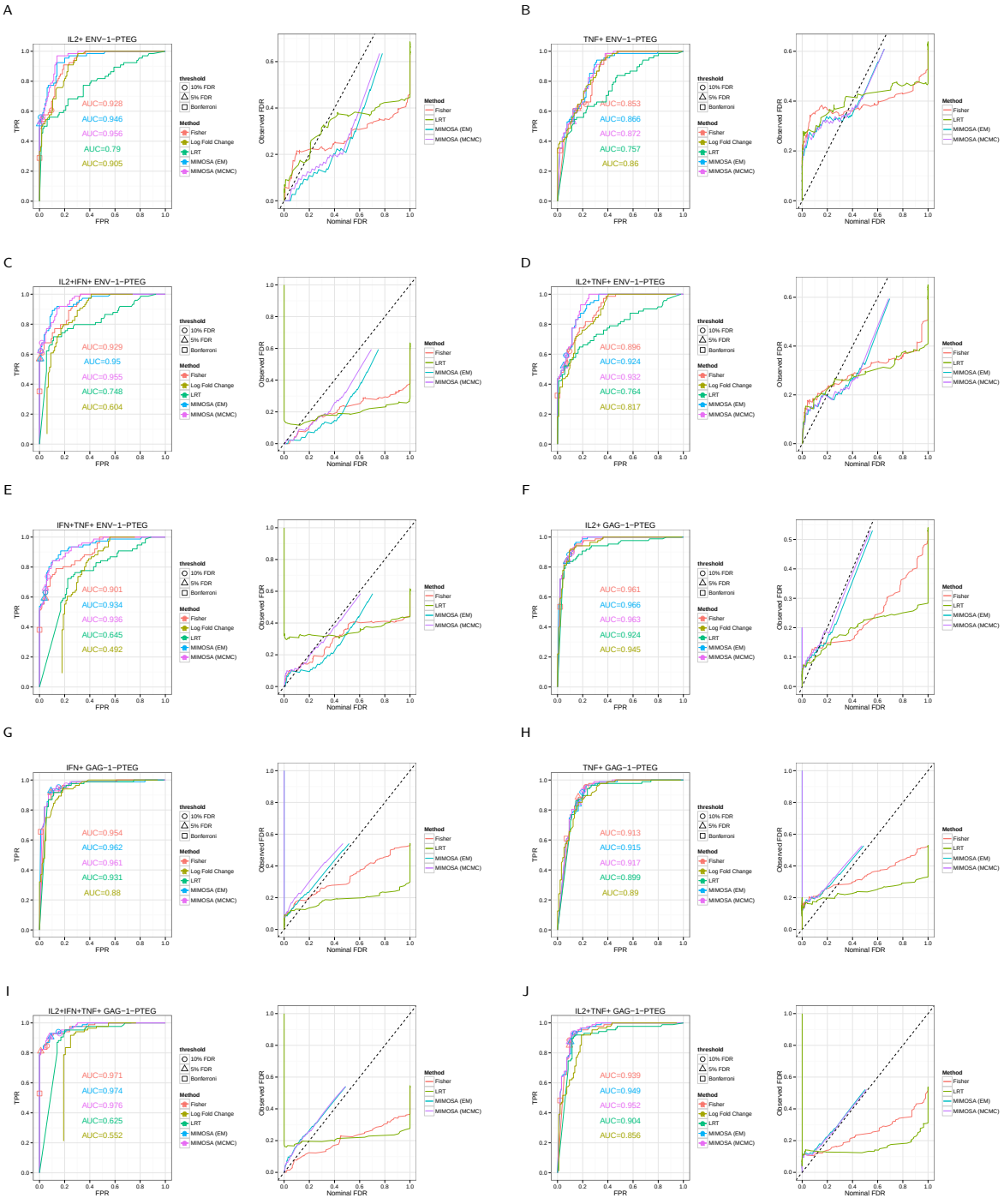

Supplementary Figure 1: Comparison of MIMOSA on other cytokines and cytokine combinations for ENV-1-PTEG and GAG-1-PTEG stimulated CD4+ T-cells from the HVTN065 trial.

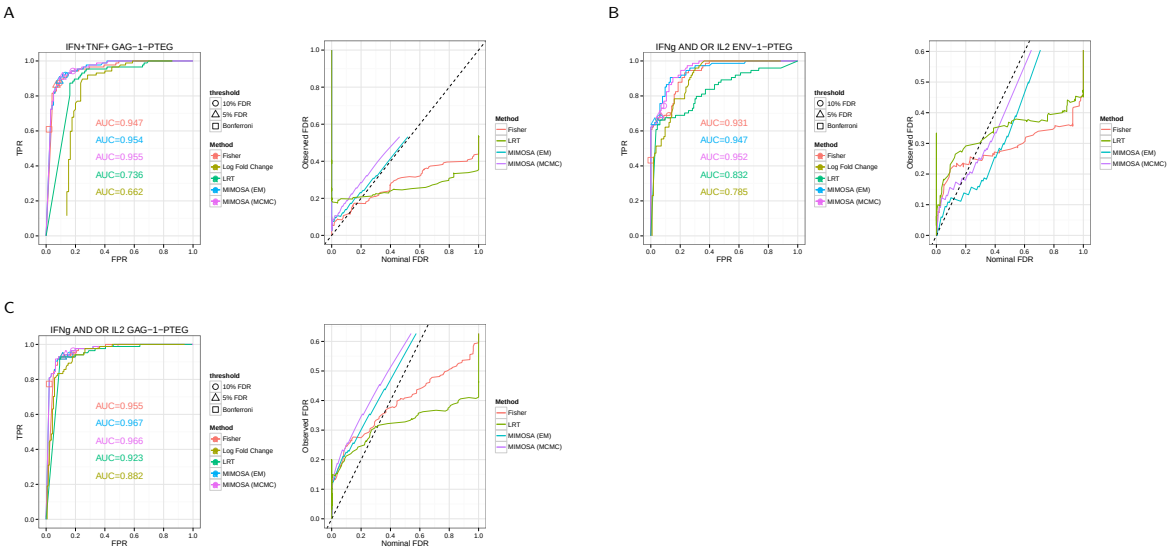

Supplementary Figure 2: Comparison of MIMOSA on other cytokines and cytokine combinations for ENV-1-PTEG and GAG-1-PTEG stimulated CD4+ T-cells from the HVTN065 trial.

References

[1] J D Altman, P A Moss, P J Goulder, D H Barouch, M G McHeyzer-Williams, J I Bell, A J McMichael, and M M Davis. Phenotypic analysis of antigen-specific T lymphocytes. *Science (New York, NY)*, 274(5284):94–96, October 1996.

[2] Michael R Betts, Martha C Nason, Sadie M West, Stephen C De Rosa, Stephen A Migueles, Jonathan Abraham, Michael M Lederman, Jose M Benito, Paul A Goepfert, Mark Connors, Mario Roederer, and Richard A Koup. Hiv nonprogressors preferentially maintain highly functional hiv-specific cd8+ t cells. *Blood*, 107(12):4781–4789, June 2006.

[3] Margaret Inokuma, Corazon dela Rosa, Charles Schmitt, Perry Haaland, Janet Siebert, Douglas Petry, Mengxiang Tang, Maria A Suni, Smita A Ghanekar, Daiva Gladding, John F Dunne, Vernon C Maino, Mary L Disis, and Holden T Maecker. Functional T cell responses to tumor antigens in breast cancer patients have a distinct phenotype and cytokine signature. *J Immunol*, 179(4):2627–2633, August 2007.

[4] K Kai McKinstry, Tara M Strutt, and Susan L Swain. The potential of CD4 T-cell memory. *Immunology*, 130(1):1–9, May 2010.

[5] H Horton, EP Thomas, JA Stucky, I Frank, Z Moodie, Y Huang, YL Chiu, MJ McElrath, and SC De Rosa. Optimization and validation of an 8-color intracellular cytokine staining (ics) assay to quantify antigen-specific t cells induced by vaccination. *Journal of immunological methods*, 323(1):39–54, 2007.

[6] Stephen C De Rosa, Fabien X Lu, Joanne Yu, Stephen P Perfetto, Judith Falloon, Susan Moser, Thomas G Evans, Richard Koup, Christopher J Miller, and Mario Roederer. Vaccination in humans generates broad t cell cytokine responses. *J Immunol*, 173(9):5372–5380, November 2004.

[7] S Plotkin. Correlates of protection induced by vaccination. *Clinical and Vaccine Immunology*, 2010.

[8] Jerome H Kim, Supachai Rerks-Ngarm, Jean-Louis Excler, and Nelson L Michael. Hiv vaccines: lessons learned and the way forward. *Current opinion in HIV and AIDS*, 5 (5):428–434, September 2010.

[9] SC Bendall, EF Simonds, P Qiu, ED Amir, PO Krutzik, R Finck, RV Bruggner, R Melamed, A Trejo, and OI Ornatsky. Single-Cell Mass Cytometry of Differential Immune and Drug Responses Across a Human Hematopoietic Continuum. *Science (New York, NY)*, 332(6030):687, 2011.

[10] Wendy L Trigona, James H Clair, Natasha Persaud, Kara Punt, Margaret Bachinsky, Usha Sadasivan-Nair, Sheri Dubey, Lynda Tussey, Tong-Ming Fu, and John Shiver. Intracellular staining for HIV-specific IFN-gamma production: statistical analyses establish reproducibility and criteria for distinguishing positive responses. *Journal of interferon & cytokine research : the official journal of the International Society for Interferon and Cytokine Research*, 23(7):369–377, July 2003.

[11] Elizabeth Sinclair, Douglas Black, C Lorrie Epling, Alexander Carvidi, Steven Z Josefowicz, Barry M Bredt, and Mark A Jacobson. CMV antigen-specific CD4+ and CD8+ T cell IFNgamma expression and proliferation responses in healthy CMV-seropositive individuals. *Viral immunology*, 17(3):445–454, 2004.

[12] M Nason. Patterns of Immune Response to a Vaccine or Virus as Measured by Intracellular Cytokine Staining in Flow Cytometry: Hypothesis Generation and Comparison of Groups. *Journal of Biopharmaceutical Statistics*, 16(4):483–498, August 2006.

[13] Michael A Proschan and Martha Nason. Conditioning in 2 x 2 tables. *Biometrics*, 65 (1):316–322, March 2009.

[14] Laurence Peiperl, Cecilia Morgan, Zoe Moodie, Hongli Li, Nina Russell, Barney S Graham, Georgia D Tomaras, Stephen C De Rosa, M Juliana McElrath, and the NIAID HIV Vaccine Trials Network. Safety and immunogenicity of a replication-defective adenovirus type 5 hiv vaccine in ad5-seronegative persons: A randomized clinical trial (hvtn 054). *PLoS ONE*, 5(10):e13579, October 2010.

[15] A.P. Dempster, N.M. Laird, and D.B. Rubin. Maximum likelihood from incomplete data via the em algorithm. *Journal of the Royal Statistical Society. Series B (Methodological)*, pages 1–38, 1977.

[16] AE Gelfand. *Markov Chain Monte Carlo in practice, edited by Gilks WR.* Richardson S., 1996.

[17] Adrian E Raftery and Steven M Lewis. [Practical Markov Chain Monte Carlo]: Comment: One Long Run with Diagnostics: Implementation Strategies for Markov Chain Monte Carlo. *STATISTICAL SCIENCE*, 7(4):493–497, November 1992.

[18] AE Raftery. Markov Chain Monte Carlo in Practice - Walter R. Gilks, Sylvia Richardson, D. J. Spiegelhalter - Google Books. *Markov chain Monte Carlo in practice*, 1996.

[19] Marcus Dittrich and Paul V Lehmann. Statistical analysis of ELISPOT assays. *Methods Mol Biol*, 792:173–183, 2012.

[20] CM Kendziorski, MA Newton, and H Lan. On parametric empirical Bayes methods for comparing multiple groups using replicated gene expression profiles - Kendziorski - 2003 - Statistics in Medicine - Wiley Online Library. *Statistics in ...*, 2003.

[21] M A Newton, C M Kendziorski, C S Richmond, F R Blattner, and K W Tsui. On differential variability of expression ratios: improving statistical inference about gene expression changes from microarray data. *Journal of Computational Biology*, 8(1): 37–52, 2001.

[22] Gordon K Smyth, Joëlle Michaud, and Hamish S Scott. Use of within-array replicate spots for assessing differential expression in microarray experiments. *Bioinformatics (Oxford, England)*, 21(9):2067–2075, May 2005.

[23] Lukas Flatz, Rahul Roychoudhuri, Mitsuo Honda, Abdelali Filali-Mouhim, Jean-Philippe Goulet, Nadia Kettaf, Min Lin, Mario Roederer, Elias K Haddad, Rafick P Sékaly, and Gary J Nabel. Single-cell gene-expression profiling reveals qualitatively distinct CD8 T cells elicited by different gene-based vaccines. *Proceedings of the National Academy of Sciences*, 108(14):5724–5729, April 2011.

[24] Jeffrey M Milush, Brian R Long, Jennifer E Snyder-Cappione, Amedeo J Cappione, Vanessa A York, Lishomwa C Ndhlovu, Lewis L Lanier, Jakob Michaëlsson, and Douglas F Nixon. Functionally distinct subsets of human NK cells and monocyte/DC-like cells identified by coexpression of CD56, CD7, and CD4. *Blood*, 114(23):4823–4831, November 2009.

[25] Nilu Goonetilleke, Stephen Moore, Len Dally, Nicola Winstone, Inese Cebere, Abdul Mahmoud, Susana Pinheiro, Geraldine Gillespie, Denise Brown, Vanessa Loach, Joanna Roberts, Ana Guimaraes-Walker, Peter Hayes, Kelley Loughran, Carole Smith, Jan De Bont, Carl Verlinde, Danii Vooijs, Claudia Schmidt, Mark Boaz, Jill Gilmour, Pat Fast, Lucy Dorrell, Tomas Hanke, and Andrew J McMichael. Induction of multifunctional human immunodeficiency virus type 1 (HIV-1)-specific T cells capable of proliferation in healthy subjects by using a prime-boost regimen of DNA- and modified vaccinia virus Ankara-vectored vaccines expressing HIV-1 Gag coupled to CD8+ T-cell epitopes. *J Virol*, 80(10):4717–4728, May 2006.